

Reynolds Addo-Akoto¹, Sang-Gil Lee¹, Jong-Seob Han², & Jae-Hung Han^{1*}

¹Korea Advanced Institute of Science and Technology, Daejeon, 34141, South Korea ²Chungnam National University, Daejeon, 34139, South Korea

Abstract

In this study, experiments are conducted to examine the aspect ratio AR and advance ratio J effects on the aerodynamic characteristics (lift, efficiency, and longitudinal force and moment) of flexible flapping. Three aspect ratios and five J cases are considered in this study. The study reveals that flexible wings can generate non-negative (≥ 0) transient lift in the upstroke for higher J cases, which is in contrast to the negative lift reported in literature for rigid wings. An increase in J decreases both the cycle-average aerodynamic lift and power irrespective of AR. Hence, a negative exponential relation is found to exist between the cycle-average lift and J, and cycle-average power and J. The AR = 1.5 and 6.0 wings are found to produce almost the same amount of lift for each change in J. Howbeit, the AR = 3.0 wing produced the best aerodynamic performance in terms of maximum lift generation and balance in efficiency. To maximize lift at mid-downstroke, the study reveals the existence of an optimum combination of J and AR. Furthermore, the resultant effect of AR and J on the forward force and pitching moment on the virtual body of the flapping flier is examined. The study reveals the tendency of low AR wings (= 1.5 and 3.0) to restore the body to its neutral position; convergence with increasing J. In addition, the low AR wings produce higher forward force than the high AR (= 6.0) wing, emphasizing the dominance and benefits of adopting a low AR wing in flapping flight applications.

Keywords: aspect ratio, advance ratio, wing flexibility (slack-angle), flapping wing, aerodynamics

1. Introduction

The flapping (back-and-forth) motion of the wings of insects and birds results in the leading-edge vortex (LEV) formation, which is the principal source of lift enhancement [1]. The LEV can be characterized based on its stability during the flapping motion. Three hypotheses so far have been presented in literature about the LEV stability; spanwise flow [1], tip vortex (TV) development [2], and rotational acceleration [3]. Although a recent study [4] has revealed that the removal and balancing of vorticity within the LEV is responsible for its stability, this can also be categorized under the spanwise flow effect. One key observation made from each study is the dependence of their findings on the aspect ratio (AR) of the wing. For instance, the TV development hypothesis is limited to AR ≤ 1.5 [5] while the vorticity balancing, spanwise flow hypothesis, scales with AR in the radial and tangential directions of the wing. Moreover, the above works were conducted with rigid-wings and the findings reveal that an optimum AR exists between 3 and 4 [6]. As AR increased, the radial limit of stall (LEV effectiveness) reduced [7]. A direct comparison of the radial limit of stall was made between rigid and flexible wings for a change in AR. It was revealed that wing flexibility further decreases the radial distance [8]. However, it was deduced that lift generation for flexible wings defined by slack-angle might not only emanate from the LEV production but also the downward acceleration of the flow and production of counter-rotating vortices due to the positive wing camber and negative wing twist, respectively [9]. Of note here is that these findings were established for

hovering flight conditions.

For forward flight motion, the dimensionless parameter, advance ratio J, is mostly used to characterize the LEV stability. This parameter stems from helicopter aerodynamics. The stand-alone effect of J on the LEV stability showed that an increase in J enhanced the vorticity production in the LEV [10]. However, an optimum J of 0.25 is reported to exist at mid-downstroke for maximum lift generation [11]. Here, the LEV behavior based on J was found to be distinct from those of AR. Howbeit, the Navier-Stokes equation presented by Lentink and Dickinson [12] for flapping wings in forward flight shows that the centripetal and Coriolis accelerations scale with $1/(J^2+1)AR$. This implies that AR and J are coupled when examining the LEV stability, which needs detailed investigation.

In this study, experiments were conducted to analyze the combinative influence of AR and J on the aerodynamic force and moment production for flexible flapping wings. An AR of 1.5, 3.0, and 6.0 and J of 0 (hovering), 0.125, 0.25, 0.5, and 1.0 were considered. The experiment was conducted in a 3-ton water tank environment with the submerged scaled-up robotic model. The model was equipped with a six-component sensor to measure the forces and moments.

2. Experimental Procedure

The flexible wing was designed based on the slack-angle concept [13]. The same material properties and design steps in ref. [13] were used in this study. The rectangular wing planform had a span length b of 250 mm, a slack-angle of 5° , and AR of 1.5, 3, and 6. Figure 1(a) shows the schematic diagram of the 3-ton water tank set-up with the forward motion of the robotic model, which represents a virtual body in the global frame coordinate system. A servo-motor was installed to tow the robotic model along the longitudinal direction. The sweep (ϕ) and pitch (α) motions were each controlled by servomotors.

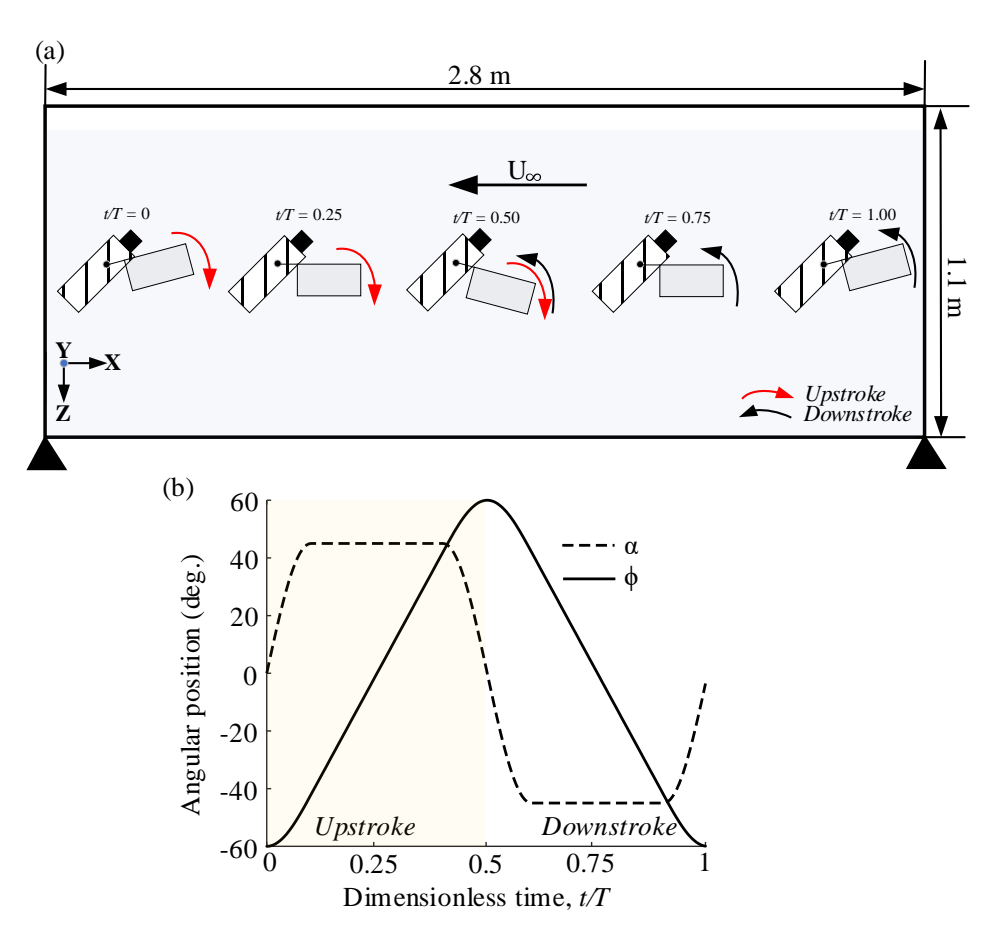


Figure 1 – (a) Schematic diagram of water-tank setup with forward flapping motion of J = 1.0 and (b) wing kinematic profile.

In Fig. 1(b), the prescribed wing motion maintained a constant angle of attack of $\pm 15^{\circ}$ from t/T = 0.1 to 0.4 in upstroke and t/T = 0.6 to 0.9 in downstroke. The total flapping time T was 10 seconds for each flapping cycle. A total of 1 to 3 continuous flapping cycles were conducted depending on the advance ratio J. The advance ratio J is defined as:

$$J = \frac{U_{\infty}}{U_t} \tag{1}$$

where the forward flight speed and cycle-average wingtip velocity are U_{∞} and $U_t = 2f\phi R$, respectively. The flapping frequency f, sweep angle ϕ , and flapping length R are 0.1 Hz, 120°, and 325 mm respectively. For hovering condition (J = 0), three flapping cycles were used while for J = 1.0, one flapping cycle was considered because the robotic model needed to travel ~1.36 m for one flapping cycle, which the length of the water tank was insufficient for more than one as shown in Fig. 1(a). Each flapping motion was repeated 21 times to assess the repeatability of the measurement and for convergence of the ensemble average. The chord-based Reynolds number Re was defined as:

$$Re = \frac{\bar{c}U_t}{v} + \frac{\bar{c}U_{\infty}}{v} = \frac{(1+J)U_t}{v} \left(\frac{b}{AR}\right)$$
 (2)

where v is the kinematic viscosity of the water (1.005 × 10⁻⁶ m²/s at 20°C). As shown in Fig. 2, the Re depended on J and AR ranging from ~0.56 × 10⁴ (J = 0 and AR = 6) to ~4.51 × 10⁴ (J = 1.0 and AR = 1.5). However, the span-based Re [14] was constant irrespective of AR and ranged from ~3.4× 10⁴ (J = 0) to ~6.8 × 10⁴ (J = 1.0). A detailed description of the scaled-up robotic model and water-tank measurement facility including the six-component force and moment sensor (Nano17-IP68, ATI automation) is provided in [15].

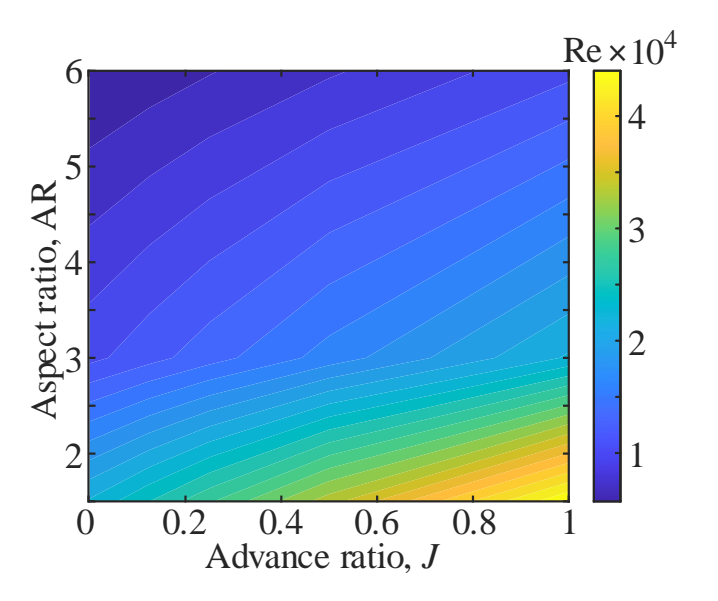


Figure 2 – Dependency of Re on AR and J.

3. Results and Discussions

3.1 Time-history aerodynamic lift depending on AR and J

Figure 3 shows the transient lift coefficient C_L for varying J at a fixed AR. The C_L was calculated as:

$$C_L = \frac{-2F_Z^B}{\rho (\hat{r}_2 U_t + J U_t)^2 b^2 / AR}$$
 (3)

where the dimensionless second radius of gyration \hat{r}_2 was 0.654 for each AR. The measured aerodynamic forces were decomposed into the adopted body-fixed coordinate system shown in Fig. 1 as the lift and drag along the Z and X directions, respectively.

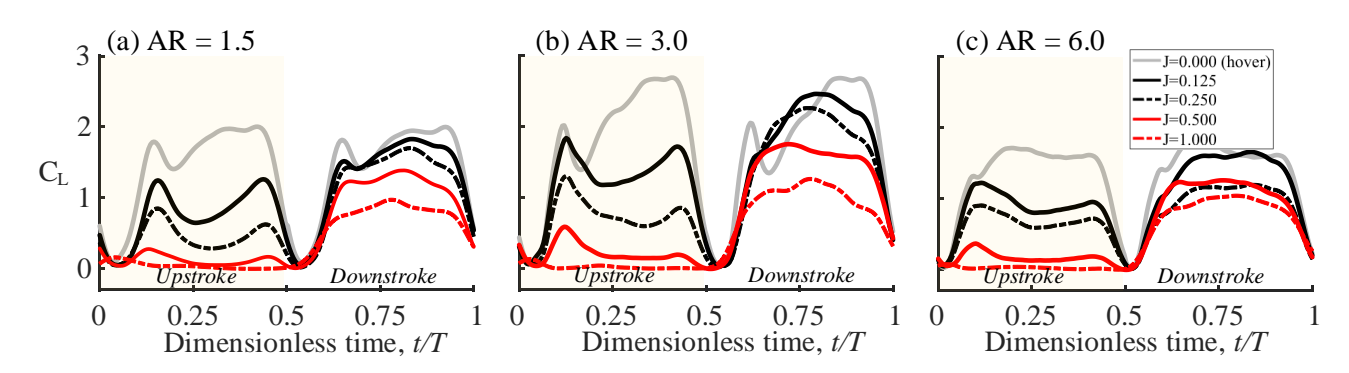


Figure 3 – Time-history lift coefficients depending on AR and *J*.

The imbalance in aerodynamic force between the upstroke and downstroke grew stronger as J increased irrespective of AR, which has already been reported in literature [10,11]. The downstroke dominated the upstroke for increasing J because of the increase in relative velocity of the wing. For J=1.0, the majority of the lift generated in the upstroke for each AR wing was near zero. The results from Han et al. [11] using the rigid wing revealed that J>0.5 produced negative lift in the upstroke. Hence, it can be deduced that wing flexibility could eliminate any possible generation of negative lift in the upstroke for higher J cases. The peak forces in the upstroke were stronger than those in the downstroke. The magnitude of the peak forces for J=0.125 was the strongest among the J cases in the upstroke. Irrespective of AR, the lift generated at the middle of upstroke decreased as J increased, which well agrees with the findings in ref. [11]. However, the effect of J on C_L at the mid-downstroke depended on AR. For AR = 1.5, the same trend in J during upstroke was observed, but for AR = 3.0, J=0.125 and 0.25 generated higher C_L than J=0 (hovering). For AR = 6.0, J=0.125 generated the same C_L at mid-downstroke with J=0 (hovering). This clearly indicates that the optimum J at mid-downstroke is strongly dependent on AR.

3.2 Cycle-average aerodynamic lift, power, and efficiency

Figure 4 shows the cycle-average (t/T = 0 to 1) aerodynamic lift and power for the change in J depending on AR. The aerodynamic power Cp and efficiency were calculated as:

$$C_P = \frac{-2(M_Z \omega_\phi + M_Y \omega_\alpha)}{\rho(\hat{r}_2 U_t + I U_t)^3 b^2 / AR} \tag{4}$$

$$Efficiency = \frac{\bar{c}_L}{\bar{c}_P}$$
 (5)

where M is the moment, ω is the angular velocity, and the bar represents average values. In Figs.

4(a) and 4(b), a negative exponential relation was observed to exist between J and average C_L and J and average C_P regardless of the AR. Howbeit, our previous study [8] revealed that this negative exponential relation exists only between AR and avera.ge C_P for both rigid and flexible wings at J=0. The increase in J produced lower cycle-average lift and power because of the observations made during upstroke as already discussed. Interestingly, AR = 1.5 and 6.0 generated almost the same amount of cycle-average lift for each J case considered. This observation agrees with our previous work [8] for J=0 and slack-angle of 5° . However, as the slack-angle changed in our previous work [8], the observation varied. Hence, the degree of wing flexibility plays a complex role in establishing such relations. The AR = 3.0 wing produced the optimum lift for each J. The AR = 3.0 rigid wing is reported to produce a balanced downwash, leading to its maximum lift generation and moderate pitching moment [16]. In addition, the LEV is reported to be stable at approximately three times the chord length along the wingspan [6,7].

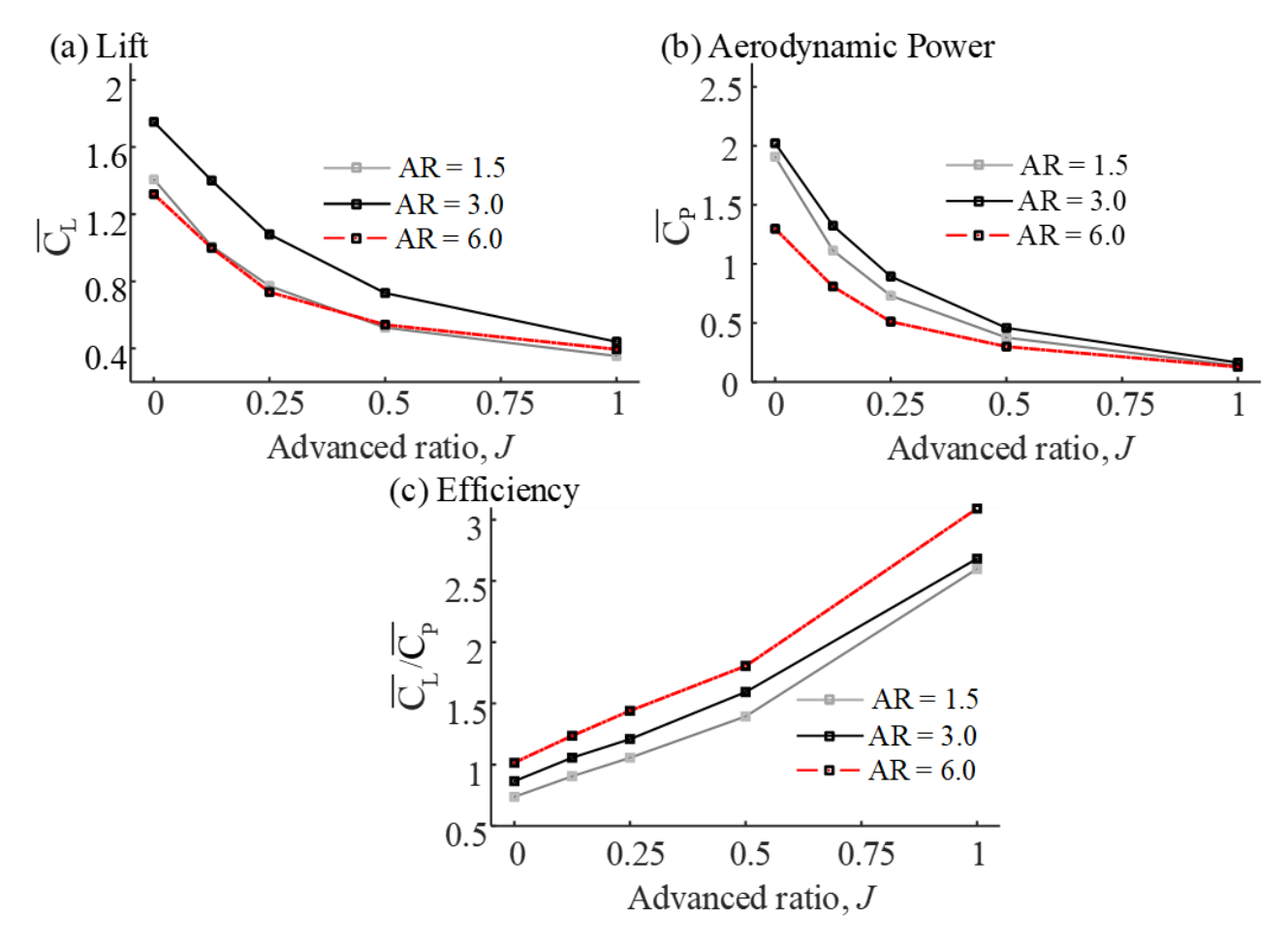


Figure 4 – Cycle-average lift, power, and efficiency based on J and AR

In Fig. 4(b), the increase in J resulted in the reduction of required aerodynamic power. Here, the AR = 3 wing required the highest power while AR = 6.0 required the least power. The AR = 1.5 wing had a balance in power requirement among the three considered AR cases. The trend in efficiency as shown in Fig. 4(c) reveals a linear relation with J, implying forward flapping flight is more economical than hovering flight. The highest AR wing of 6.0 in this study was the most efficient among the AR cases due to the lowest power requirement although relatively generated lower lift. The AR = 3 wing produced the maximum lift and relatively better efficiency, making it the best-performing wing among the considered AR cases.

3.3 Relation between AR and J at the mid-downstroke

In section 3.1, the detailed discussion about lift coefficient characteristics depending on J and AR was discussed. In this section, the instantaneous values at mid-downstroke were extracted, and a contour plot is presented in Fig. 5 to have a better observation of the relation between AR and J in this study. An optimum lift generation is observed for 0 < J < 0.25 and 2.0 < AR < 4.0. An optimum J of 0.25 is reported using a rigid wing but this study shows that wing flexibility reduces the J below 0.25 but higher than J = 0. This indirectly suggests the appropriate J and AR selection for lift optimization for slack-angled flapping wing micro aerial vehicles (FWMAVs) wing design.

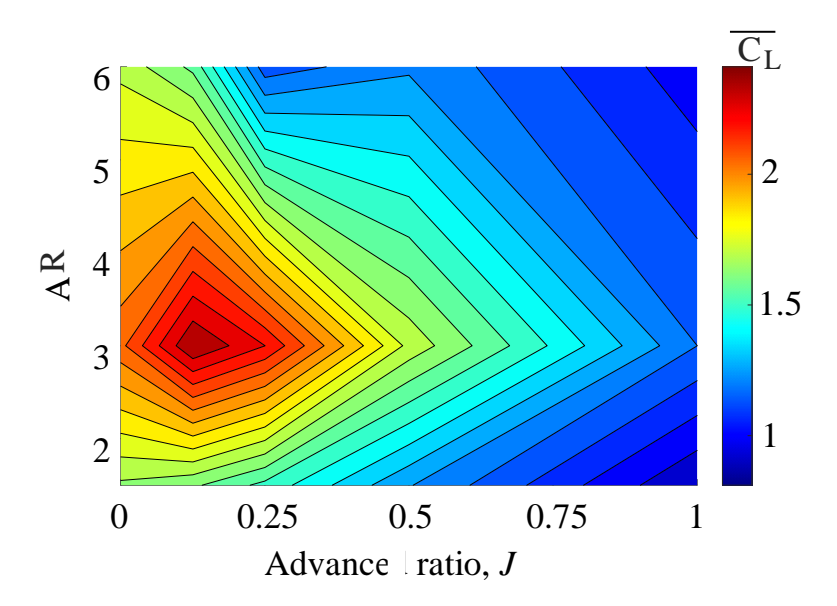


Figure 5 – Relation between AR and J for optimum lift generation at mid-downstroke.

3.4 Effect of AR and J on body forward force and pitch moment

3.4.1 Aerodynamic characteristics

Figure 6 shows the measured aerodynamic force and moment coefficients in the longitudinal direction. Similar to Eqn. (3), the forward force $C_{F_X}^{\ \ B}$ and pitching moment $C_{M_Y}^{\ \ B}$ acting on the body were respectively calculated as:

$$C_{F_X}{}^B = \frac{2F_X{}^B}{\rho(\hat{r}_2 U_t + J U_t)^2 b^2 / AR} \tag{6}$$

$$C_{F_X}{}^B = \frac{2F_X{}^B}{\rho(\hat{r}_2 U_t + J U_t)^2 b^2 / AR}$$

$$C_{M_Y}{}^B = \frac{2M_Y{}^B}{\rho(\hat{r}_2 U_t + J U_t)^2 b^2 / AR}$$
(6)

as J varied. However, as the AR increased, the notable distinctions were minimized especially during upstroke. Unlike the C_L plots that showed some level of unsteadiness during upstroke, the C_{Fv}^B plot displayed some level of steadiness for the AR = 3.0 and 6.0 wings. This indicates the possibility of predicting steady-state aerodynamic forces using the quasi-steady aerodynamic modeling approach. In addition, the level of unsteadiness in C_L stemmed from the axial force component [18]. For J = 1.0, the wing showed some tendency to generate forward force compared to the other J cases that produced backward force. For the moment coefficients, a general observation of the pitching up-and-down of the wing in each half-stroke was made. A contradicting observation to $C_{F_X}^{\ \ B}$ was found where an increase in AR rather resulted in the notable distinction for the effect of J.

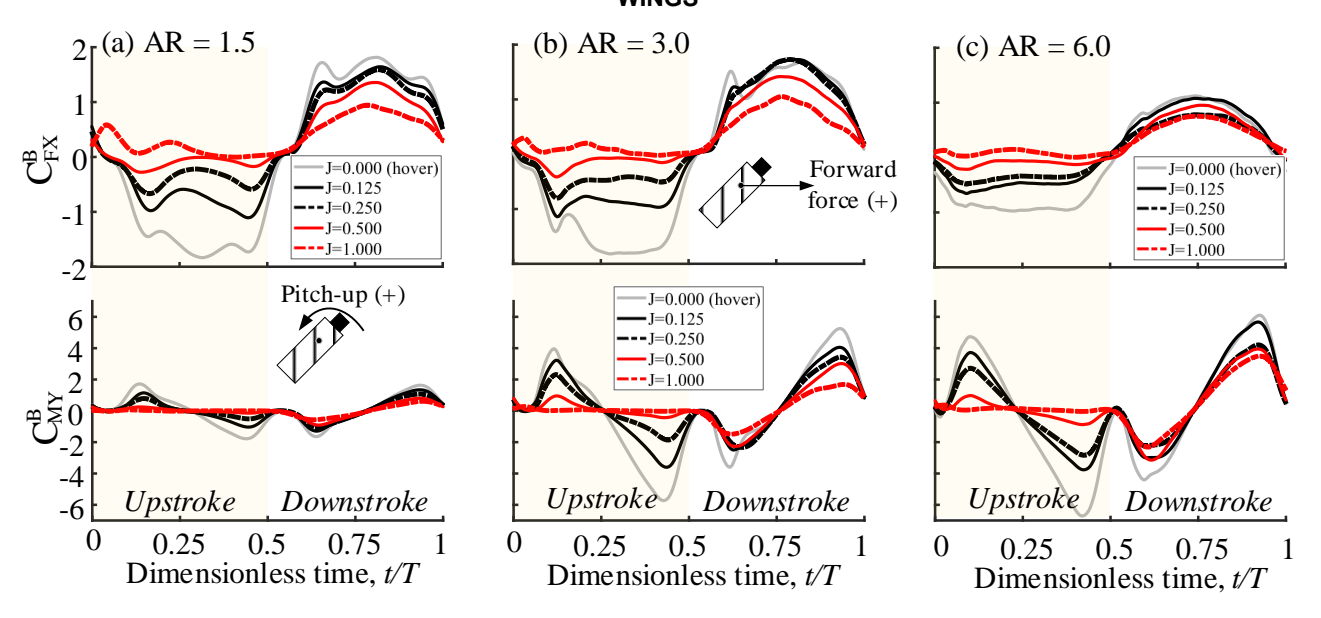


Figure 6 – Time-history body forward force and pitching moment for each AR wing as J varies.

3.4.2 Cycle-average

The resultant effect of the change in AR and J on the behavior of the virtual body was examined. Figure 7 shows the cycle-average force and moment coefficient values. For hovering (J=0), each AR wing produced a resultant backward force. The AR wing of 1.5 produced the highest forward force in most cases except for J=0.50. The difference in forward force production between AR of 1.5 and 3 for J>0 was less than 5%. But, between AR = 1.5 and 6.0 was around 22%, indicating the supremacy of low AR wings (AR \leq 3.0) in flapping wing aerodynamics. The AR = 6.0 wing showed divergence towards the neutral position while the AR = 1.5 and 3.0 wings showed convergence tendencies. This further confirms the tendency of the low AR wings to restore the body to its neutral position under forward flight conditions.

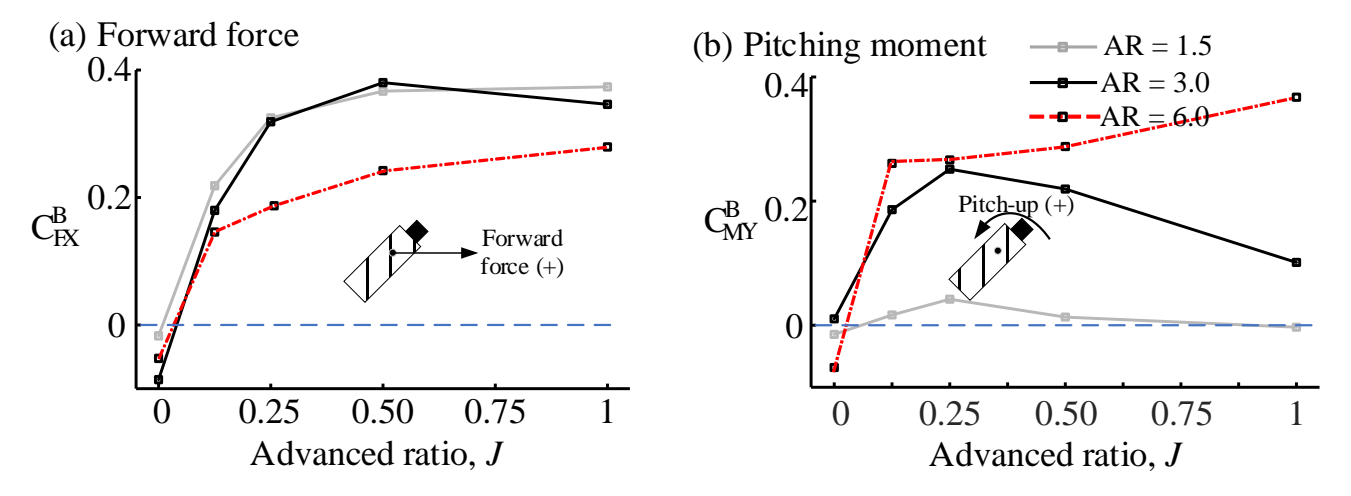


Figure 7 – Cycle-average force and moment coefficients based on *J* for a change in AR.

4. Conclusion

The combinative effects of aspect ratio AR and advance ratio J on the aerodynamic characteristics (lift, efficiency, and longitudinal force and moment) of flexible flapping wing are examined. The

experiments were conducted in a water-tank measurement facility for a 5° slack-angled wing of AR = 1.5, 3.0, and 6.0 with J of 0 (hovering) to 1.0. In this study, the peak forces in the upstroke were stronger than those in the downstroke. At higher J, the flexible AR wings produced non-negative transient lift, which contradicts that of rigid wings in literature. This shows some peculiar advantages of wing flexibility in flapping aerodynamics. Also, irrespective of AR, the lift generated at the midupstroke reduced as J increased. Contrarily, the effect of J on the lift coefficient was strongly dependent on AR at mid-downstroke. The AR wing of 3.0 generated the highest lift and was reasonably efficient for all considered J cases. The low AR wings of 1.5 and 3.0 produced sufficiently higher forward force with the display of tendencies to return the body of the flier to its neutral position. This restoration of the body to its neutral position was seen to diverge for AR = 6.0 wing with increasing J.

5. Acknowledgments

This research was supported by the Unmanned Vehicles Core Technology Research and Development Program through the National Research Foundation of Korea (NRF) and Unmanned Vehicle Advanced Research Center (UVARC) funded by the Ministry of Science and ICT, the Republic of Korea (2020M3C1C1A01083415).

6. Contact Author Email Address

Reynolds Addo-Akoto: reykoto@kaist.ac.kr
Sang-Gil Lee: sanggil.lee@kaist.ac.kr
Jong-Seob Han: jongseobhan@cnu.ac.kr

Jae-Hung Han (Corr. Author): jaehunghan@kaist.ac.kr

7. Copyright Statement

The authors confirm that they, and/or their company or organization, hold copyright on all of the original material included in this paper. The authors also confirm that they have obtained permission, from the copyright holder of any third-party material included in this paper, to publish it as part of their paper. The authors confirm that they give permission, or have obtained permission from the copyright holder of this paper, for the publication and distribution of this paper as part of the ICAS proceedings or as individual off-prints from the proceedings.

References

- [1] Ellington CP, Den Van Berg C, Willmott AP and Thomas ALR. Leading-edge vortices in insect flight. *Nature*, Vol. 384, No. 6610, pp 626–630, 1996.
- [2] Birch JM and Dickinson MH. Spanwise flow and the attachment of the leading-edge vortex on insect wings. *Nature*, Vol. 412, No. 6848, pp 729–733, 2001.
- [3] Lentink D and Dickinson MH. Rotational accelerations stabilize leading edge vortices on revolving fly wings. *Journal Experimental Biology*, Vol. 212, No. 16, pp 2705–2719, 2009.
- [4] Chen L, Wang L, Zhou C, Wu J and Cheng B. Effects of Reynolds number on leading-edge vortex formation dynamics and stability in revolving wings. *Journal of Fluid Mechanics*, Vol. 931, No. A13, pp 1–23, 2022.
- [5] Ringuette MJ, Milano M and M., "Role of the tip vortex in the force generation of low-aspect-ratio normal flat plates," *Journal of Fluid Mechanics*, Vol. 581, pp 453–468, 2007.
- [6] Jardin T and Colonius T. On the lift-optimal aspect ratio of a revolving wing at low Reynolds number. *Journal of Royal Society Interface*, Vol. 15, No. 143, pp 20170933, 2018.
- [7] Kruyt JW, Van Heijst GJF, Altshuler DL and Lentink D. Power reduction and the radial limit of stall delay in

- revolving wings of different aspect ratio. Journal of Royal Society Interface, Vol. 12, No. 105, 2015.
- [8] Addo-Akoto R, Han JS and Han JH. Aerodynamic characteristics of flexible flapping wings depending on aspect ratio and slack angle. *Physics of Fluids*, Vol. 34, No. 5, 2022.
- [9] Addo-Akoto R, Yang HH, Han JS and Han JH. Wing flexibility effect on aerodynamic performance of different flapping wing planforms. *Journal of Fluids and Structures*, Vol. 123, No. September, pp 104006, 2023.
- [10] Harbig RR, Sheridan J and Thompson MC. The role of advance ratio and aspect ratio in determining leading-edge vortex stability for flapping flight. *Journal of Fluid Mechanics*, Vol. 751, pp 71–105, 2014.
- [11] Han JS, Chang JW and Han JH. The advance ratio effect on the lift augmentations of an insect-like flapping wing in forward flight. *Journal of Fluid Mechanics*, Vol. 808, pp 485–510, 2016.
- [12] Lentink D and Dickinson MH. Biofluiddynamic scaling of flapping, spinning and translating fins and wings. *Journal Experimental Biology*, Vol. 212, No. 16, pp 2691–2704, 2009.
- [13] Addo-Akoto R, Han JS and Han JH. Aerodynamic performance of flexible flapping wings deformed by slack angle. *Bioinspiration and Biomimetics*, Vol. 15, No. 6, 2020.
- [14] Harbig RR, Sheridan J and Thompson MC. Reynolds number and aspect ratio effects on the leading-edge vortex for rotating insect wing planforms. *Journal of Fluid Mechanics*, Vol. 717, pp 166–192, 2013.
- [15] Han JS, Nguyen AT and Han JH. Aerodynamic characteristics of flapping wings under steady lateral inflow. *Journal of Fluid Mechanics*, Vol. 870, pp 735–759, 2019.
- [16] Han JS, Chang JW and Cho HK. Vortices behavior depending on the aspect ratio of an insect-like flapping wing in hover. *Experiments in Fluids*, Vol. 56, No. 9, pp 1–16, 2015.
- [17] Han J.S. Interaction of the wakes of two flapping wings on control forces and moment. Aerospace Science and Technology, Vol. 115, pp 106794, 2021.
- [18] Addo-Akoto R, Han JH and Han JS. Effects of sweep-motion profile on rigid and flexible flapping-wing aerodynamics. *In AIAA SCITECH Forum*, Virtual Event, pp 1–14, 2021.